HOKKAIDO UNIVERSITY

Title	Phonon modes in a Möbius band
Author(s)	Nishiguchi, Norihiko; Wybourne, Martin
Citation	Journal of Physics Communications, 2(8), 85002 https://doi.org/10.1088/2399-6528/aad49b
Issue Date	2018-08-01
Doc URL	https://hdl.handle.net/2115/71261
Rights(URL)	https://creativecommons.org/licenses/by/3.0/
Type	journal article
File Information	Nishiguchi_2018_J._Phys._Commun._2_085002.pdf

Hokkaido University Collection of Scholarly and Academic Papers : HUSCAP

Journal of Physics Communications

PAPER • **OPEN ACCESS**

Phonon modes in a Möbius band

To cite this article: Norihiko Nishiguchi and Martin N Wybourne 2018 *J. Phys. Commun.* **2** 085002

View the article online for updates and enhancements.

This content was downloaded by nishiguchi from IP address 133.87.123.217 on 02/08/2018 at 01:08

Journal of Physics Communications

OPEN ACCESS

RECEIVED
5 June 2018

REVISED
9 July 2018

ACCEPTED FOR PUBLICATION
19 July 2018

PUBLISHED
1 August 2018

Original content from this work may be used under the terms of the Creative Commons Attribution 3.0 licence.

Any further distribution of this work must maintain attribution to the author(s) and the title of the work, journal citation and DOI.

PAPER

Phonon modes in a Möbius band

Norihiko Nishiguchi[1,3] **and Martin N Wybourne**[2]

[1] Division of Applied Physics, Hokkaido University, Sapporo 060-8628, Japan
[2] Department of Physics and Astronomy, Dartmouth College, Hanover, NH 03755, United States of America
[3] Author to whom any correspondence should be addressed.

E-mail: nn@eng.hokudai.ac.jp **and** martin.n.wybourne@dartmouth.edu

Keywords: phonon modes, Möbius strip, topology

Abstract

It is well known that phonon modes become sensitive to the geometry of an object when the phonon wavelengths are comparable to the objects physical length scale. In contrast, the sensitivity of phonon modes toward topology is much less explored and understood. In this paper we discuss the effects of topology on phonon modes using a finite thickness Möbius band of centerline radius a as the model system. The phonon modes are derived using the xyz algorithm based on Riemannian geometry. From the boundary conditions and parity we identify two sets of modes with wave numbers $q = n/2a$ described by odd and even integers n. Modes characterized by odd integers have flexural vibrations whereas those characterized by even integers exhibit dilatational and shear/torsional motion. While the phonon dispersion at large wave numbers agrees with that of structures having simple topology (rings and wires), at low frequencies and wave numbers the Möbius topology introduces significant differences. Uniquely, we find three of the four phonon branches do not go to zero frequency with decreasing wave number, but converge on a finite frequency. We identify a new form of vibrational pattern resembling incomplete breathing modes and discuss the ramifications of the modified spectrum, including a local increase in the density of states and the existence of a phonon band gap.

1. Introduction

Möbius strip topology has fascinated artists and scientists since the middle of the nineteenth century when the structure was first identified by Listing and Möbius [1–4]. The mechanical properties, equilibrium shape and surface geometry of this unique one-sided, single-boundary structure have been studied extensively [5, 6]. In addition, a rich variety of research associated with the topology has been reported, including the stability of soap films [7], novel light polarization schemes [8], numerical calculations of Laplace-Beltrami eigenfunctions [9], and birdcage resonators that show half-integer harmonic behavior when configured as a Möbius strip [10]. Techniques have been developed to fabricate three-dimensional nanostructures with nontrivial topology [11–14] and the effects of topology on electron transport behavior [15–18] discussed. More generally, the consequence of topology, and the concept of topological order, has been the subject of extensive research on correlated electron systems, such as the fractional quantum Hall effect [19] and topological insulators [20, 21].

At the nanoscale, geometric constraints give rise to phenomena related to phonon confinement, such as specific heat anomalies [22–24], the quantization of thermal conductance [25, 26], and modifications to the Raman spectra of nano-crystalline materials [27]. The importance of low-frequency flexural modes on the thermal and mechanical properties of graphene sheets has been comprehensively studied [28], and tuning the flexural mode by modifying the geometry of graphene nano-ribbons has been considered as a means to control transport properties [29]. Also, the thermal conductivity has been shown to depend on topology, with Möbius strips displaying a lower conductivity than rings or ribbons; a result attributed to increased phonon-phonon scattering and localization [30].

In this paper we address the effect of topology on phonon modes in the elastic continuum regime. We derive the vibrational spectra of a finite thickness Möbius strip modeled as a rectangular cross-section bar that is twisted

© 2018 The Author(s). Published by IOP Publishing Ltd

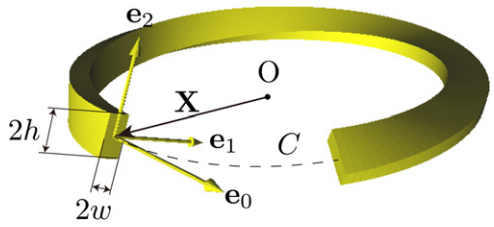

Figure 1. Möbius band and Coordinate system.

axially by π radians and is formed into a continuous structure by linking the ends. The centerline of the structure is assumed to be a perfect circle of radius a. For clarity, we term this model structure a Möbius band for the remainder of the paper. We do not consider chirality because it does not play a role in the phonon properties of individual, isolated Möbius bands. We first set up the model for the band and derive related structural parameters, such as the metric tensors and Christoffel symbols based on Riemannian geometry. We consider the parity and boundary conditions for phonon modes specific to a Möbius band, and find an unusual coexistence of two classes of phonon mode with allowed wavelengths of $2\pi a$ divided by either integers or half integers. Following previous work [31], the phonon modes are derived using the xyz-algorithm [32] reformulated in terms of Riemann geometry. We introduce a set of basis functions satisfying the boundary conditions in order to express the phonon mode displacements. A critical consideration is the need for displacement vector matching imposed by the π radian twist of a Möbius band. Comparing the calculated modes to those of a wire and a ring, we find the lowest frequency dispersion branches close to the zone center for a Möbius band have strikingly different characteristics. In the case of a wire (ring), four (two) branches converge to a frequency $\omega = 0$ as the wave number approaches zero. We show that for a Möbius band, one branch has $\omega = 0$ at the zone center while three branches converge around a finite frequency ω_g at zero wave vector. The density of states is enhanced around ω_g below which the spectral density becomes very low, giving rise to a phonon band gap not found in other closed structures, for example rings. Details of the phonon spectra close to the zone center are shown to be sensitive to elasticity, but insensitive to geometry. We discuss these sensitivities and conclude that topology rather than geometry is the dominant factor determining the low-frequency phonon spectrum of a Möbius band.

2. Möbius band and coordinate system

We consider a Möbius band modeled as a rectangular cross-section bar of single crystal that is twisted axially by π radians and is formed into a continuous structure by linking the ends as shown figure 1. The center line C denoted by the dashed line is assumed to be a perfect circle of radius a.

We first introduce a coordinate system which rotates along C. $\mathbf{X}$ denotes a position on C and s is a length between the position and prescribed origin on C. $\mathbf{t}$, $\mathbf{n}$ and $\mathbf{b}$ are the tangential unit vector along C, the normal vector defined below, and the unit vector perpendicular to $\mathbf{t}$ and $\mathbf{n}$. κ is the curvature and τ is the torsion. All of these are defined and related by the following Frenet-Serrete formulae;

$$\begin{cases} \mathbf{t} &= \mathbf{e}_0 = \dfrac{d}{ds}\mathbf{X}(s) \\ \dfrac{d\mathbf{t}}{ds} &= \dfrac{d}{ds}\mathbf{e}_0 = \kappa\mathbf{n} \\ \kappa &= \left|\dfrac{d}{ds}\mathbf{t}\right| = \left|\dfrac{d}{ds}\mathbf{e}_0\right| \\ \mathbf{b} &= \mathbf{t}\times\mathbf{n} \\ \dfrac{d\mathbf{n}}{ds} &= -\kappa\mathbf{t} + \tau\mathbf{b} \\ \dfrac{d\mathbf{b}}{ds} &= -\tau\mathbf{n} \end{cases} \tag{1}$$

$\mathbf{n}$ indicates the center of circle and the curvature becomes $\kappa = 1/a$. $\mathbf{b}$ indicates the direction normal to the circle, independent of s, so that $\tau = 0$.

Using $\mathbf{n}$ and $\mathbf{b}$, we introduce a frame comprised of $\mathbf{e}_0 \equiv \mathbf{t}$ and two unit vectors $\mathbf{e}_1$ and $\mathbf{e}_2$ which rotate with increasing s along C. Assuming a constant rate of rotation of the frame and putting $\theta = s/2a$, we define the unit vectors rotating with increasing s by

$$\begin{pmatrix} \mathbf{e}_1 \\ \mathbf{e}_2 \end{pmatrix} = \begin{pmatrix} \cos\theta & -\sin\theta \\ \sin\theta & \cos\theta \end{pmatrix} \begin{pmatrix} \mathbf{n} \\ \mathbf{b} \end{pmatrix}. \tag{2}$$

Supposing that the Möbius band is made of material having a cubic crystal structure, for example copper or gold, the unit vectors $\mathbf{e}_0$, $\mathbf{e}_1$ and $\mathbf{e}_2$ are set to be parallel to each crystal axis.

To describe the structure and equation of motion of elasticity in terms of Riemannian geometry, the position in the Möbius band is given by

$$\mathbf{r} = \mathbf{X}(x^0) + x^1\mathbf{e}_1(x^0) + x^2\mathbf{e}_2(x^0) \tag{3}$$

Following the usual convention, superscript of x^j indicates the j th component of the contravariant vector, where $x^0 \equiv s$. The subscript of x_j denotes the j th component of the covariant vector. Considering the rectangular cross section of $2w \times 2h$ connected to the rotating frame as shown in figure 1, the variable ranges are

$$-w \leqslant x^1 \leqslant w,\ -h \leqslant x^2 \leqslant h,\ 0 \leqslant x^0 \leqslant 2\pi a. \tag{4}$$

For the system to be physically feasible, the half-wide w and half-height h should satisfy the condition $\kappa \max(w, h) < 1$.

Geometric parameters such as the metric tensors g_{ij} and Christoffel symbols Γ_{ijk} are given by

$$g_{ij} \equiv \partial_i\mathbf{r} \cdot \partial_j\mathbf{r} \tag{5}$$

$$\Gamma_{ijk} \equiv \frac{1}{2}(\partial_k g_{ij} + \partial_j g_{ki} - \partial_i g_{jk}), \tag{6}$$

which are summarized in appendix.

3. XYZ algorithm

The xyz algorithm developed by Visscher [32] is a powerful method to numerically obtain vibrational modes of a free-standing object. That work showed that the equation of motion of vibrations for a free-standing object becomes the same as the wave equation in a bulk material and that the exact solution automatically satisfies the boundary condition for a free surface. In the present work, we apply the method to a Möbius band. Since the method was originally developed in terms of Euclidean geometry, we reformulate the method using Riemannian geometry [33] .

To begin, we introduce contravariant and covariant displacement vectors u^i and u_i which are related by

$$u_i = g_{ij}u^j. \tag{7}$$

The strain tensor ε_{ij} is defined by

$$\varepsilon_{ij} = \frac{1}{2}(\nabla_j u_i + \nabla_i u_j), \tag{8}$$

where $\nabla_j u_i$ means covariant derivative of u_i with respect to x^j estimated by

$$\nabla_j u_i = \partial_j u_i - \Gamma^k_{ji}u_k. \tag{9}$$

Assuming Hooke's law, the stress tensor σ^{ij} is associated with ε_{ij} via the stiffness tensor C^{ijkl} as

$$\sigma^{ij} = C^{ijkl}\varepsilon_{kl} = C^{ijkl}\nabla_k u_l. \tag{10}$$

Using the strain and stress tensors, the Lagrangian of a Möbius band yields

$$L = \int\left(\frac{\rho\dot{u}_i\dot{u}^i}{2} - \frac{\nabla_i u_j \sigma^{ij}}{2}\right)\sqrt{g}\,dx^0dx^1dx^2, \tag{11}$$

where $\sqrt{g}$ represents the Jacobian and $g = |g_{ij}|$. From the variational principle and boundary condition for a free surface, we have the following equation for a phonon mode with frequency ω

$$\rho\omega^2 u^i + \nabla_j\sigma^{ij} = 0. \tag{12}$$

We express the displacement vector, using a series of bases Φ_λ;

$$u^i = \sum_\lambda \chi^i_\lambda \Phi_\lambda(x^0, x^1, x^2), \tag{13}$$

where

$$\Phi_\lambda(x^0, x^1, x^2) = \left(\frac{x^1}{w}\right)^l \left(\frac{x^2}{h}\right)^m e^{iqx^0} \tag{14}$$

and λ stands for $\lambda = \{l, m, q\}$ ($l, m \geqslant 0$). In order to set up an equation to obtain the coefficients χ^i_λ, we first substitute equations (13) into (12) and multiply by the complex conjugate of $\Phi_{\lambda'}$. Integrating over the volume, we have

$$\sum_\lambda \chi^j_\lambda \int_V [\rho\omega^2 g_{ij}\Phi^*_{\lambda'}\Phi_\lambda - (g_{ik}\partial_l\Phi^*_{\lambda'} + \Gamma_{kli}\Phi^*_{\lambda'})C^{klmn}(g_{mj}\partial_n\Phi_\lambda + \Gamma_{mnj}\Phi_\lambda)] \times \sqrt{g}\,dx^0dx^1dx^2 = 0. \tag{15}$$

Defining matrix elements $E_{i\lambda';j\lambda}$ and $F_{i\lambda';j\lambda}$ as

$$E_{i\lambda';j\lambda} \equiv \int_V \rho g_{ij}\Phi^*_{\lambda'}\Phi_\lambda \sqrt{g}\,dx^0dx^1dx^2 \tag{16}$$

$$F_{i\lambda';j\lambda} \equiv \int_V (g_{ik}\partial_l\Phi^*_{\lambda'} + \Gamma_{kli}\Phi^*_{\lambda'})C^{klmn}(g_{jm}\partial_n\Phi_\lambda + \Gamma_{mnj}\Phi_\lambda)\sqrt{g}\,dx^0dx^1dx^2, \tag{17}$$

Equation (15) is reformulated to be the following secular equation

$$\omega^2 \sum_\lambda E_{i\lambda';j\lambda}\chi^j_\lambda = \sum_\lambda F_{i\lambda';j\lambda}\chi^j_\lambda. \tag{18}$$

Numerically solving equation (18), we obtain phonon spectra of Möbius bands and corresponding displacement vectors.

4. Parity and boundary condition

Each phonon mode component has a certain parity for inversion of coordinates x^1 and x^2 associated with structural symmetries. Because of the π radian twist in a Möbius band, the parity will also depend on matching the displacement vectors around the band. Since bases are closely related to the parity, we examine the boundary condition to choose a suitable set of bases.

As x^0 changes from 0 to $4\pi a$ along the centerline C, the frame rotates axially around $\mathbf{e}_0$ by 2π radians and returns to the original orientation. Then the displacement vector matches itself at the original position, in other words all the phonon modes have a period of $4\pi a$;

$$u^i(0, x^1, x^2) = u^i(4\pi a, x^1, x^2). \tag{19}$$

In addition, since the frame rotates by π radians when x^0 increases from 0 to $2\pi a$, the displacement vector at $(x^0 = 0, x^1, x^2)$ coincides with that at $(x^0 = 2\pi a, -x^1, -x^2)$. The frame rotation also inverts displacement components u^1 and u^2. Putting these things together, we have the following boundary conditions for displacement components;

$$u^0(0, x^1, x^2) = u^0(2\pi a, -x^1, -x^2) \tag{20}$$

$$u^1(0, x^1, x^2) = -u^1(2\pi a, -x^1, -x^2) \tag{21}$$

$$u^2(0, x^1, x^2) = -u^2(2\pi a, -x^1, -x^2). \tag{22}$$

Supposing an asymptotic case of extremely large radius in comparison with wavelength $\lambda/a \ll 1$, the phonon modes of a Möbius band will closely resemble those of a rectangular wire as understood from equation (18), which in the limit of $a \to \infty$ reduces to the secular equation for phonon modes in a rectangular wire [31]. A rectangular wire supports four kinds of phonon modes; a dilatational mode referred to as mode I, two flexural modes referred to as modes II and III, and shear/torsional modes referred to as mode IV. The shear and torsional modes are clearly separated only for a square wire, but are mixed for a rectangular wire. The displacement components of these modes are given by

$$u^j_{\mathrm{M}} = \sum_{s,t\geqslant 0} \chi^j_{\mathrm{M};stn}\left(\frac{x^1}{w}\right)^{2s+l}\left(\frac{x^2}{h}\right)^{2t+m} e^{iqx^0}, \tag{23}$$

where l and m are 0 or 1, giving spatial symmetry of each displacement component. The combinations (l, m) for phonon modes are summarized in table 1. Here we apply the boundary conditions on the phonon modes in a rectangular wire. Putting equations (23) into (19), we have a condition for wave number q as

$$4\pi aq = 2n\pi, \tag{24}$$

Table 1. Spatial symmetry (l, m) of phonon modes.

Mode:M	u^0	u^1	u^2
I	(0, 0)	(1, 0)	(0, 1)
II	(0, 1)	(1, 1)	(0, 0)
III	(1, 0)	(0, 0)	(1, 1)
IV	(1, 1)	(0, 1)	(1, 0)

where n is an integer. The wave number q is discretized to be an integer multiple of $1/2a$

$$q = \frac{n}{2a}. \tag{25}$$

Since u^i changes its sign only for an odd n when x^0 changes from 0 to $2\pi a$, we have the parity for change in x^0 as

$$u^i(0, x^1, x^2) = (-1)^n u^i(2\pi a, x^1, x^2). \tag{26}$$

Considering inversions of x^1 and x^2, we have

$$u^i(2\pi a, x^1, x^2) = (-1)^{l+m} u^i(2\pi a, -x^1, -x^2). \tag{27}$$

Putting equations (27) into (26), we have the following relationship of the displacement;

$$u^i(0, x^1, x^2) = (-1)^{l+m+n} u^i(2\pi a, -x^1, -x^2). \tag{28}$$

Comparing equation (28) with equations (20)–(22), it is found that the sum of powers $N = l + m + n$ for each component must satisfy

$$N = \text{even for } u^0 \tag{29}$$

$$N = \text{odd for } u^1 \tag{30}$$

$$N = \text{odd for } u^2. \tag{31}$$

When n is an odd number(n_{odd}), $l + m$ becomes odd for u^0 and even for u^1 and u^2, and vice versa. As seen from table 1, modes II and III satisfy (29)–(31) only for n_{odd}, and modes I and IV satisfy the conditions only when n is an even number (n_{even}) including 0.

From the relationship between the wave number and wavelength $q = 2\pi/\lambda$ and equation (25), the wavelength is given by the circumference $2\pi a$ divided by $n/2$ as

$$\lambda = \frac{2\pi a}{n/2}. \tag{32}$$

When $n = 0$, the wavelength becomes infinite and the vibrations become uniform motions. Considering both n_{odd} and n_{even} are possible for phonon modes in Möbius bands, modes II and III have a wavelength of the circumference divided by a half-integer while modes I and IV have that divided by an integer. It is unusual that the wavelength of modes II and III becomes a non-integer multiple of length for closed(ring-like) structures and that two different sets of phonon modes alternate as the wave number changes by $1/2a$. These unusual properties are specific to phonon modes of Möbius bands.

As the ratio λ/a increases, the curvature and torsion of a Möbius band will gradually modify or couple the phonon modes. Modifications of phonon modes from those of wire will be most important in the low frequency region near the zone center when the wavelengths become comparable to, or larger than, the circumference of a Möbius band, as shown below.

5. Phonon modes in a Möbius band

5.1. Phonon spectra

Numerically solving the secular equation (18), we illustrate in figure 2 the phonon spectra of a Möbius band of copper whose cross sectional dimensions are $(2w/a) \times (2h/a) = 0.1 \times 0.2$. The solid circles denote the spectra of phonon modes composed of modes I and IV at $q = n_{\text{even}}/2a$, and open circles indicate the spectra of phonon modes composed of modes II and III at $q = n_{\text{odd}}/2a$. The solid lines are the dispersion relations of phonon modes I, II, III and IV in a rectangular wire of the same cross-section, which are distinguished by colors. At high frequencies, the Möbius band phonon spectra show substantial agreement with the optical[4] and acoustic

[4] The optical branches are analogous to confined optical modes found in thin sheets, nanowires, and nanocrystals, which have been widely explored by Raman spectroscopy. We note the associated Brillouin zone-center band gaps depend on physical dimensions.

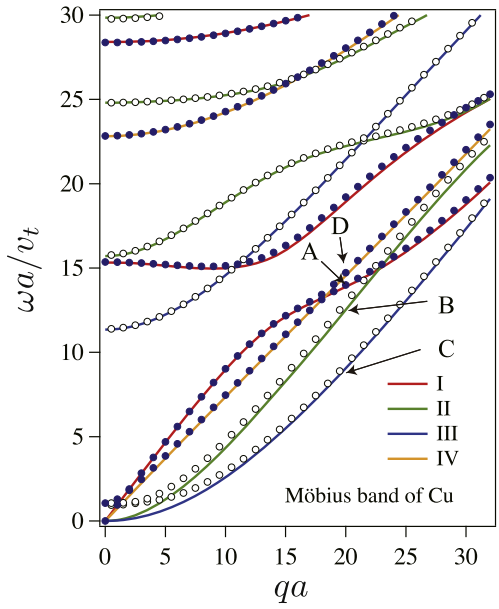

Figure 2. Phonon frequencies versus wave number of a copper Möbius band with cross sectional dimensions $(2w/a) \times (2h/a) = 0.1 \times 0.2$. The solid circles and open circles indicate phonon spectra at wave number q of an integer and half-integer multiple of $1/a$, respectively. The solid lines are the dispersion relations of phonon modes in a rectangular wire of copper with the same cross section area as Möbius band. Four different kinds of modes referred to as I, II, III and IV are distinguished by colors. Vibrational patterns at four points labelled A, B, C, and D are examined below. The used material parameters are $\rho = 8.94$ g/cm^3, $C_{11} = 168.4$ GPa, $C_{12} = 121.4$ GPa, $C_{44} = 75.4$ GPa [].

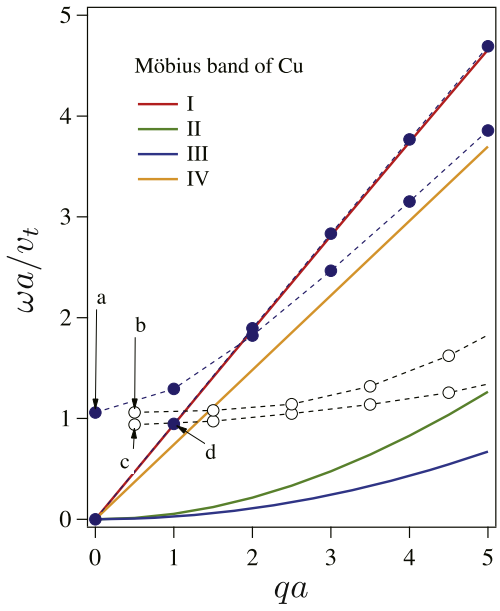

Figure 3. Phonon spectra of a copper Möbius band in the low frequency region near the zone center of figure 2. Points labelled a, b, c and d indicate characteristic frequencies of Möbius band. See the text.

phonon dispersion branches of a wire. In contrast, and of primary interest, at low frequency and wave number the acoustic phonon branches disagree markedly with the dispersion relations of a wire.

Figure 3 is a magnified region of figure 2 revealing the detailed spectral distribution of the acoustic branches in the low frequency region near the zone center, and introduces four characteristic frequencies $\omega_a, \omega_b, \omega_c$ and ω_d. A noticeable feature is that the frequencies of the two lowest branches associated with modes II and III for $qa < 10$ deviate significantly from the parabolic dispersion relations of a wire and have finite magnitudes of the characteristic frequencies (figure 3) ω_b and ω_c, which are comparable to $\omega_g \approx v_t/a$ at small wave numbers. Here v_t is the sound velocity of transverse waves defined by $v_t = \sqrt{C_{44}/\rho}$. The frequencies ω_b and ω_c at $qa = 0.5$ can be

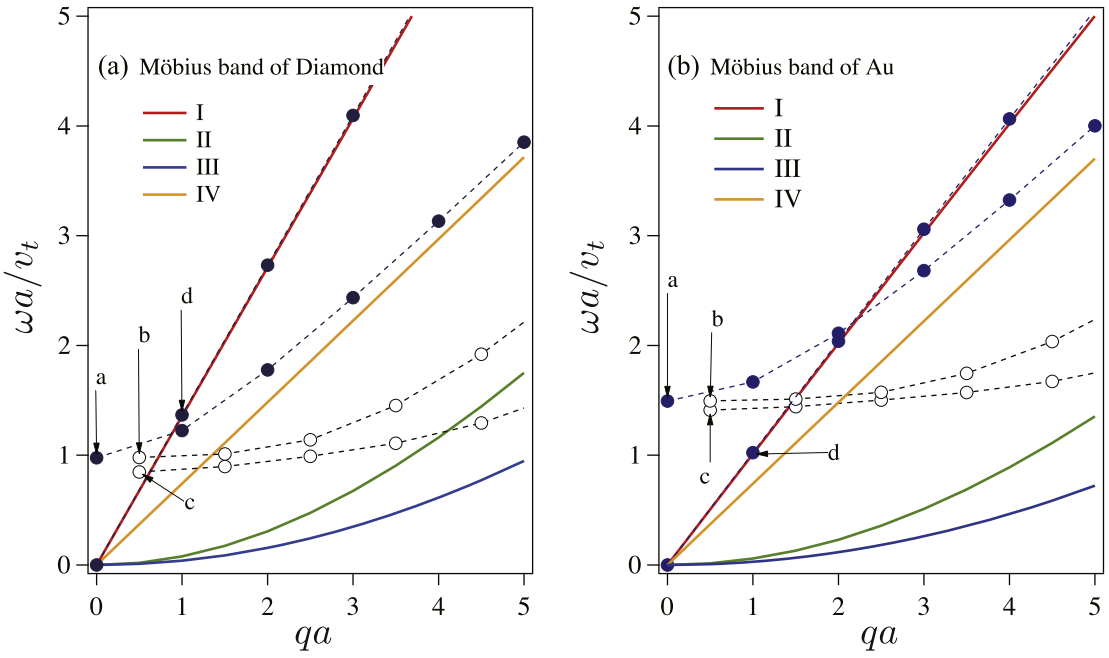

Figure 4. Phonon spectra of (a) diamond and (b) gold Möbius bands in the low frequency region near the zone center. The cross sectional dimensions are the same as those of a copper Möbius band. The solid lines are the dispersion relations of a rectangular wire of diamond and gold, respectively. Points labelled a, b, c and d indicate characteristic frequencies of Möbius bands. The material parameters of diamond are $\rho = 3.53$ g/cm^3, $C_{11} = 1075.0$ GPa, $C_{12} = 139.3$ GPa, $C_{44} = 567.2$ GPa and those of gold are $\rho = 19.49$ g/cm^3, $C_{11} = 201.6$ GPa, $C_{12} = 169.7$ GPa, $C_{44} = 45.4$ GPa [34].

shown to be $\omega_b = \sqrt{C_{11}/2\rho a^2}$ and $\omega_c = \sqrt{C_{11}/2\rho a^2}\,[1 - O(\frac{w^2+h^2}{a^2})]$ by solving the secular equation (18) including only the relevant acoustic phonon modes. We note that because $C_{11} \approx 2C_{44}$ for copper, ω_g and $\omega_{b,c}$ coincide accidentally.

The spectra associated with mode IV also deviate from the linear dispersion relation of a wire and the frequencies become larger than those of mode I, where the frequency ω_a at $q = 0$ is estimated as $\omega_a = \sqrt{C_{11}/2\rho a^2}$. On the other hand, the spectra associated with mode I almost coincide with the linear dispersion relation of a wire and the frequency at $qa = 1$ is estimated as $\omega_d = \sqrt{Y/\rho a^2}$ where Y is Young's modulus, which is given by $Y = C_{11} - 2C_{12}^2/(C_{11} + C_{12})$ for cubic materials. For copper, ω_c is the minimum of these frequencies, and as there are no modes with a lower finite frequency a band gap of characteristic frequency ω_c occurs.

In order to consider the details of the band gap we note that ω_a, ω_b and ω_c depend on C_{11}, but only ω_d depends on Young's modulus suggesting that ω_d could possibly be lower than ω_a, ω_b and ω_c for materials other than copper. To parametrize the posibility of a band gap, we introduce the ratio of ω_d and ω_b

$$f \equiv \frac{\omega_d}{\omega_b} = \left[2 - \frac{4C_{12}^2}{C_{11}(C_{11} + C_{12})}\right]^{1/2}. \tag{33}$$

For materials with $f \geqslant 1$ a phonon band gap exists with modes II, III, and IV providing a high density of states around ω_b and ω_c, below which the spectral density is low. For materials with $f < 1$, mode I becomes the lowest non-zero energy state, somewhat analogous to having a state in the gap. Although ω_c would be better than ω_b for the definition of f, we use ω_b instead of ω_c since it is too complicated to express ω_c in a compact form. Aside from the case that ω_d falls between ω_b and ω_c like copper, f is a useful parameter to judge the occurrence of a phonon frequency gap. With $f = 1.05$ for aluminum and 1.18 for diamond, we have confirmed the frequency gaps numerically, as shown in figure 4(a) for diamond. On the other hand, gold ($f = 0.82$) has a mode with finite frequency below ω_d as shown in figure 4(b).

Here we mention the dependence of these characteristic frequencies on the Möbius band thickness and width. The frequencies ω_a, ω_b, ω_c and ω_d are tolerant to changes of the cross sectional dimensions, although at higher wavenumbers the slopes of spectra of modes II and III depend strongly on thickness. It is apparent, therefore, that the fundamental properties of the frequency gap do not change with the geometry, suggesting they are characteristic of the topology.

Furthermore, we note that the frequency gap does not appear for other closed structures such as rings. Phonon modes of rings are derived by using the boundary condition $u^i(0, x^1, x^2) = u^i(2\pi a, x^1, x^2)$. Although

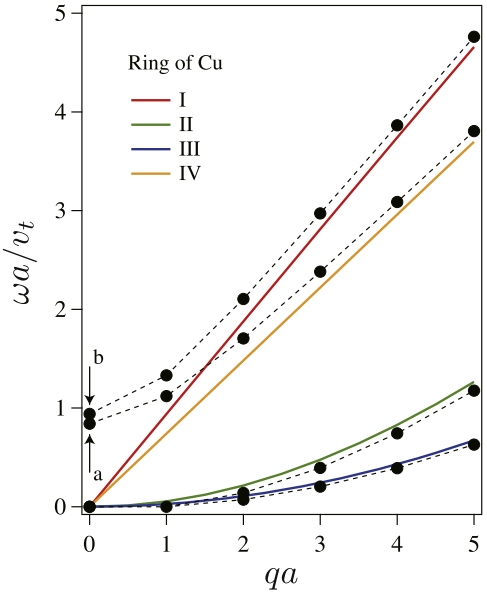

Figure 5. Phonon spectra of a copper ring with the same cross sectional dimensions as the Möbius band. The solid circles indicate frequencies versus wave number and only have an integer multiples of $1/a$.

the high wave number phonon spectra of a ring agree well with the dispersion relations of wires, similar to the case for the Möbius bands, the ring spectra deviate from those of wire in the low frequency region. However, unlike the Möbius band the ring does not have a frequency gap since the spectra of the two lowest branches are almost the same as modes II and III of wires and tend to $\omega = 0$ with decreasing wave number, as shown in figure 5 [35, 36]. This further supports the conclusion that the frequency gap is a phenomenon characterisitc of the Möbius band topology.

5.2. Vibrational patterns

From the finding that the phonon spectra of a Möbius band match the dispersion relations of wires at high frequencies or large wave numbers, we expect that the vibrational patterns of Möbius bands will also resemble those of wires. Figure 6 shows vibrational patterns at points A, B, C and D denoted in figure 2. It is apparent that they exhibit dilatational(A), torsional(D) and flexural motions(B and C) corresponding to those in the rectangular wire [31]. Here we pay attention to B and C whose wavelengths are $\lambda = 2\pi a/(19/2)$. We may say that the twisted structure of Möbius bands absorbs or compensates for the phase difference caused by the half of wavelength, making such a wavelength realizable.

Vibrational motions of modes at low frequencies are more specific to the Möbius band. Figure 7 shows vibrational patterns for modes (a) at $q = 0$, (b) and (c) at $qa = 1/2$ and (d) at $qa = 1$ denoted in figures 3 and 4. Because of gentle spatial variations of displacement vectors for small wave numbers, the arrows express the dynamical motions. Mode (a) exhibits uniform axial-torsion along the circumference. Although the motion is common to the torsional mode of wire, the frequency ω_a is finite, as is the case for phonon modes in a ring referred to as 'torsional modes' in reference [36] (see figure 8(a)). Mode (d) is longitudinal waves whose wavelength matches the circumference $\lambda = 2\pi a$, and leads to a mode with $\omega = 0$ at $q = 0$. Thus the motion as well as the spectra coincide with mode I of wires. We note that a ring does not support such a mode leading to $\omega = 0$. The vibrational patterns of modes (b) and (c) at $qa = 1/2$ with $\lambda = 4\pi a$ show new forms of vibration that resemble incomplete breathing motions, which are in contrast to the breathing mode of a ring shown in figure 8(b).

6. Summary and discussions

The phonon modes in a Möbius band with finite thickness have been derived. The Möbius band has been modeled as a rectangular bar axially twisted by π radians whose ends are perfectly linked. The phonon spectra and corresponding displacement vectors are obtained by means of the xyz-algorithm that we have extended in terms of Riemannian geometry. As a result of mode parity and boundary conditions, we find that a Möbius band supports two distinct sets of allowed phonon wavelengths characterized by odd and even integers. The wavelengths are given by $\lambda = 2\pi a/(n/2)$, with odd integers corresponding to flexural modes II and III, and even

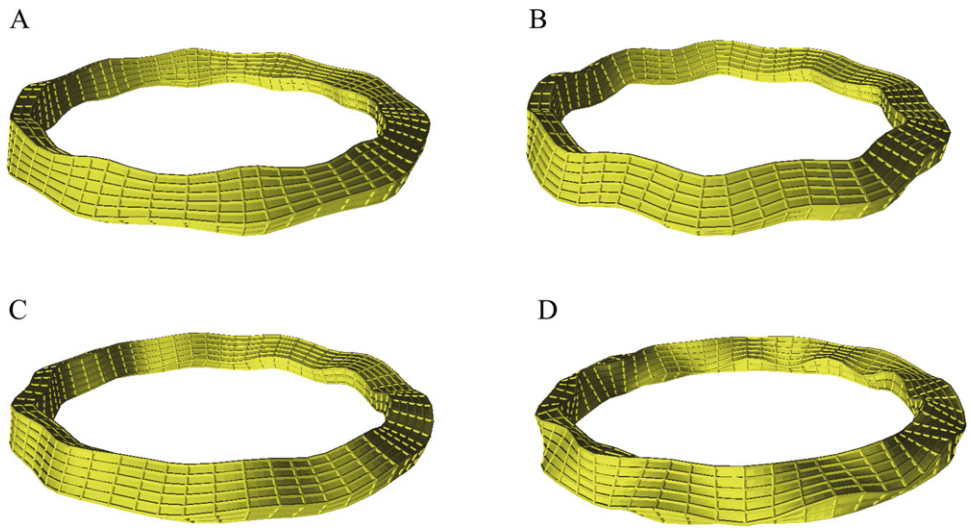

Figure 6. Vibrational patterns at A, B, C and D denoted in figure 2. The wavelengths of A and D are $\lambda = 2\pi a/10$ and those of B and C are $\lambda = 2\pi a/9.5$. For vibrational pattern B (C), the displacement occurs primarily in the direction of the longer (shorter) edge of the cross section. Compared with B, C can be considered to be more like the flexural vibrations of a thin-plate, therefore having a vibration frequency lower than that of B.

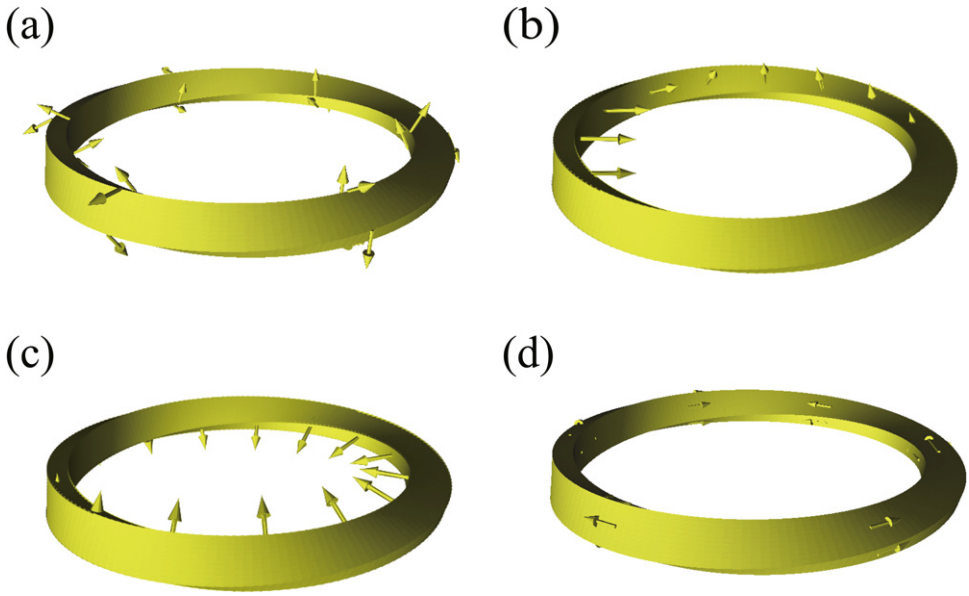

Figure 7. Vibrational patterns at (a)–(d) denoted in figures 3 and 4. The arrows indicate the directions of displacement vectors. Modes (b) and (c) have a period of $4\pi a$.

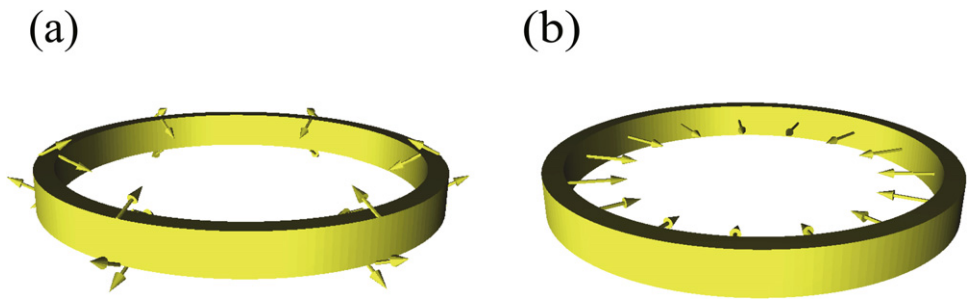

Figure 8. Vibrational patterns of modes in a ring at (a) and (b) denoted in figure 5. The arrows indicate the directions of displacement vectors, showing (a) a uniform torsional motion and (b) a breathing motion.

integers to dilatational and shear/torsional modes I and IV. Importantly, this leads to integer and half-integer wavelength relationships being allowed, with the lowest frequency flexural mode ($n = 1$) having a wavelength of twice the center line circumference and the lowest finite frequency dilatational mode ($n = 2$) having a wavelength equal to the circumference. It also follows that the nature of the modes alternate as the wave number changes by $1/2a$. A structure that supports modes with integer and half-integer wavelength relationships is unusual and is a direct consequence of the nontrivial topology.

We have also shown that phonon modes with wavelengths much shorter than the center-line circumference coincide with the dilatational, shear/torsional and two flexural modes of a rectangular wire. In this limit the vibrational patterns closely match those of wires, with the twisted structure of a Möbius band accounting for the half of wavelength phase difference. Major differences between phonon spectra of the Möbius band, wire and ring appear in the low frequency region near the zone center. For the Möbius band, three of the four acoustic branches do not go to $\omega = 0$ with decreasing wave number; instead they converge toward a finite frequency around which the number of states locally increases giving rise to the possibility of a phonon band gap. We have addressed the robustness if the gap towards geometry and have noted that a gap does not occur in other closed structures, such as rings that have two branches with $\omega = 0$ at $q = 0$. We have parameterized details of the gap in terms of characteristic frequencies that depend on the elasticity of the material. Similar to other mechanisms that modify the phonon spectral distribution, we expect that the distorted spectral distribution resulting from the topology will give rise to anomalous thermal properties, which will be discussed elsewhere.

Finally, we emphasize that the topology plays a significant role in the phonon modes. The phonon band gap is one of the significant characteristics caused by the Möbius topology. Finite systems, such as nano particles, also have phonon spectral gaps. In these cases the band gap is caused by phonon confinement, which is a size dependent effect [24]. Very interestingly, a ring does not have a phonon band gap in spite of the finite size since the lowest acoustic branch begins at $\omega = 0$ and increases parabolically with respect to wavenumber. The difference in spectra between the nano particles and rings is caused by the difference in topology, i.e. the existence of a hole. Likewise, the difference between the Möbius bands and rings is also due to the difference in topology, i.e. twisted or not-twisted. Thus, topology substantially affects the phonon modes in a finite system and introduces effects that are comparable with, or larger than, those originating from geometry.

Acknowledgments

We would like to express our appreciation to Miles P Blencowe for his helpful comments.

Appendix. Geometric parameters associated with Möbius band

Using the derivatives of position vector (3) with respect to x^i

$$\frac{\partial \mathbf{r}}{\partial x^0} = (1 - \kappa_j x^j)\mathbf{e}_0 + \psi x^1 \mathbf{e}_2 - \psi x^2 \mathbf{e}_1 \tag{A.1}$$

$$\frac{\partial \mathbf{r}}{\partial x^1} = \mathbf{e}_1 \tag{A.2}$$

$$\frac{\partial \mathbf{r}}{\partial x^2} = \mathbf{e}_2, \tag{A.3}$$

where

$$\psi \equiv -\frac{d\theta}{dx^0}, \tag{A.4}$$

g_{ij} becomes

$$(g_{ij}) = \begin{pmatrix} \gamma^4 + \psi^2|x|^2 & -\psi x^2 & \psi x^1 \\ -\psi x^2 & 1 & 0 \\ \psi x^1 & 0 & 1 \end{pmatrix} \tag{A.5}$$

where

$$|x|^2 = (x^1)^2 + (x^2)^2 \tag{A.6}$$

and

$$\gamma \equiv \sqrt{1 - \kappa_j x^j}. \tag{A.7}$$

The determinant g of geometric tensor is obtained as

$$g = det\,(g_{ij}) = \gamma^4, \tag{A.8}$$

and the contravariant metric tensor is derived as follows;

$$(g^{ij}) = \gamma^{-4}\begin{pmatrix} 1 & \psi\, x^2 & -\psi\, x^1 \\ \psi\, x^2 & \gamma^4 + \psi^2 (x^2)^2 & -\psi^2 x^1 x^2 \\ -\psi\, x^1 & -\psi^2 x^1 x^2 & \gamma^4 + \psi^2 (x^1)^2 \end{pmatrix}. \tag{A.9}$$

For Christoffel symbols of the first kind, we have

$$\Gamma_{000} = 2\,\gamma^4 \beta_0 \tag{A.10}$$
$$\Gamma_{001} = \Gamma_{010} = 2\,\gamma^4 \beta_1 + \psi^2 x^1 \tag{A.11}$$
$$\Gamma_{002} = \Gamma_{020} = 2\,\gamma^4 \beta_2 + \psi^2 x^2 \tag{A.12}$$
$$\Gamma_{100} = -2\,\gamma^4 \beta_1 - \psi^2 x^1 \tag{A.13}$$
$$\Gamma_{102} = \Gamma_{120} = -\psi \tag{A.14}$$
$$\Gamma_{200} = -2\,\gamma^4 \beta_2 - \psi^2 x^2 \tag{A.15}$$
$$\Gamma_{201} = \Gamma_{210} = \psi \tag{A.16}$$
$$\Gamma_{ijk} = 0 \qquad \text{otherwise}, \tag{A.17}$$

where β_n is defined by

$$\beta_n \equiv \frac{1}{\gamma}\frac{\partial \gamma}{\partial x^n}, \tag{A.18}$$

and estimated, respectively, as

$$\beta_0 = \frac{\psi(-\kappa_2 x^1 + \kappa_1 x^2)}{2(1 - \kappa_j x^j)} \tag{A.19}$$
$$\beta_1 = \frac{-\kappa_1}{2(1 - \kappa_j x^j)} \tag{A.20}$$
$$\beta_2 = \frac{-\kappa_2}{2(1 - \kappa_j x^j)}. \tag{A.21}$$

Christoffel symbols of the second kind are derived from

$$\Gamma^l{}_{mn} \equiv g^{lk}\Gamma_{kmn}, \tag{A.22}$$

and we have

$$\Gamma^0{}_{00} = 2(\beta_0 - \psi x^2 \beta_1 + \psi x^1 \beta_2) \tag{A.23}$$
$$\Gamma^0{}_{01} = \Gamma^0{}_{10} = 2\beta_1 \tag{A.24}$$
$$\Gamma^0{}_{02} = \Gamma^0{}_{20} = 2\beta_2 \tag{A.25}$$
$$\Gamma^1{}_{00} = 2\psi x^2(\beta_0 - \psi x^2 \beta_1 + \psi x^1 \beta_2) - 2\,\gamma^4 \beta_1 - \psi^2 x^1 \tag{A.26}$$
$$\Gamma^1{}_{01} = \Gamma^1{}_{10} = 2\psi x^2 \beta_1 \tag{A.27}$$
$$\Gamma^1{}_{02} = \Gamma^1{}_{20} = 2\psi x^2 \beta_2 - \psi \tag{A.28}$$
$$\Gamma^2{}_{00} = -2\psi x^1(\beta_0 - \psi x^2 \beta_1 + \psi x^1 \beta_2) - 2\,\gamma^4 \beta_2 - \psi^2 x^2 \tag{A.29}$$
$$\Gamma^2{}_{01} = \Gamma^2{}_{10} = -2\,\psi x^1 \beta_1 + \psi \tag{A.30}$$
$$\Gamma^2{}_{02} = \Gamma^2{}_{20} = -2\,\psi x^1 \beta_2 \tag{A.31}$$
$$\Gamma^i{}_{jk} = 0 \qquad \text{otherwise}. \tag{A.32}$$

ORCID iDs

Norihiko Nishiguchi https://orcid.org/0000-0001-5899-830X

References

[1] Listing J B 1862 Der census räumlicher complexe oder verallgemeinerung des euler'schen satzes von den polyëdern *Abhandlungen der Königlichen Gesellschaft der Wissenschaften in Göttingen* **10** 97–182

[2] Möbius A F 1865 Ueber die bestimmung des inhaltes eines polyëders *Berichte über die Verhandlungen der Königlich Sächsischen Gesellschaft der Wissenschaften Mathematischphysikalische Klasse* **17** 31–68
[3] Gallier J and Xu D 2013 *A Guide to the Classification theorem for Compact Surfaces Geometry and Computing* 9 (Berlin Heidelberg: Springer) (https://doi.org/10.1007/978-3-642-34364-3)
[4] Emmer M 1980 *Visual Art and Mathematics: The Moebius Band Leonardo* **13** 108–11
[5] Fosdick R and Fried E 2015 *The Mechanics of Ribbons and Möbius Bands* (Berlin: Springer)
[6] Starostin E L and van der Heijden G H M 2007 The shape of a Möbius Strip *Nat. Mater.* **6** 563
[7] Goldstein R E, Moffatt H K, Pesci A I and Ricca Renzo L 2010 Soap-film Möbius strip Changes topology with a twist singularity *PNAS* **107** 21979–84
[8] Bauer T, Banzer P, Karimi E, Orlov S, Rubano A, Marrucci L, Santamato E, Boyd R W and Leuchs G 2015 Observation of optical polarization Möbius strips *Science* **347** 934
[9] MacDonald C B, Brandman J and Ruuth S J 2011 Solving eigenvalue problems on curved surfaces using the closest point method *J. Comput. Phys.* **230** 7944–56
[10] Ballon D J and Voss H U 2008 Classical Möbius-ring resonators exhibit fermion-boson rotational symmetry *Phys. Rev. Lett.* **101** 247701
[11] Arora W J, Nichol A J, Smith H I and Barbastathis G 2006 Membrane folding to achieve three-dimensional nanostructures: nanopatterned silicon nitride folded with stressed chromium hinges *Appl. Phys. Lett.* **88** 053108
[12] Tanda S, Tsuneta T, Okajima Y, Inagaki K, Yamaya K and Hatakenaka N 2002 Crystal topology: a Möbius strip of single crystals *Nature* **417** 397–8
[13] Tanda S, Tsuneta T, Toshima T, Matsuura T and Tsubota M 2005 Topological crystals *J. Physique IV* **131** 289–94
[14] Dongran H, Suchetan P, Yan L and Hao Y 2010 Folding and cutting DNA into reconfigurable topological nanostructures *Nat. Nanotechnol.* **5** 712–7
[15] Gravesen J and Willatzen M 2005 Eigenstates of Möbius Nanostructures Including Curvature Effects *Phys. Rev.* A **72** 032108
[16] Korte A P and van der Heijden G H M 2009 Curvature-induced electron localization in developable Möbius-like nanostructures *J. Phys.: Condens. Matter* **21** 495301
[17] Pylypovskyi O V, Kravchuk V P, Sheka D D, Makarov D, Schmidt O G and Gaididei Y 2015 Coupling of chiralities in spin and physical spaces: the Möbius ring as a case study *Phys. Rev. Lett.* **114** 197204
[18] Hayashi M and Ebisawa H 2001 Little-parks oscillation of superconducting Möbius strip *J. Phys. Soc. Japan* **70** 3495–8
[19] Wen X-G 1995 Topological orders and edge excitations in fractional quantum Hall states *Adv. Phys.* **44** 405–73
[20] Hasan M Z and Kane C L 2010 Colloquium: topological insulators *Rev. Mod. Phys.* **82** 3045–67
[21] Manoharan H C 2010 Topological Insulators: a romance with many dimensions *Nat. Nanotechnol.* **5** 477–9
[22] Novotny V, Meincke P P M and Watson J H P 1972 Effect of size and surface on the specific heat of small lead particles *Phys. Rev. Lett.* **28** 901–3
[23] Baltes H P and Hilf E R 1973 Specific heat of lead grains *Solid State Commun.* **12** 369–73
[24] Nishiguchi N and Sakuma T 1981 Vibrational spectrum and specific heat of fine particles *Solid State Commun.* **38** 1073–7
[25] Schwab K, Henriksen E A, Worlock J M and Roukes M L 2010 Measurement of the quantum of thermal conductivity *Nature* **44** 974
[26] Rego L G C and Kirczenow G 1998 Quantized thermal conductance of dielectric quantum wires *Phys. Rev. Lett.* **81** 232
[27] Arora A K, Rajalakshmi M and Ravindran T R 2004 Phonon confinement in nanostructured materials *Encyclopedia of Nanoscience and Nanotechnology* **8** 499–512
[28] Jiang J W, Wang B S, Wang J S and Park H S 2015 A review on the flexural mode of graphene: lattice dynamics, thermal conduction, thermal expansion, elasticity and nanomechanical resonance *J. Phys.: Condens. Matter* **27** 083001
[29] Yang N, Jiang J W and Li B 2012 How does folding modulate the thermal conductivity of graphene? *Appl. Phys. Lett.* **100** 093107
[30] Jiang J W, Wang J S and Li B 2010 Topological effect on thermal conductivity in graphene *J. Appl. Phys.* **108** 064307
[31] Nishiguchi N, Ando Y and Wybourne M N 1997 Acoustic phonon modes of rectangular quantum wires *J. Phys.: Condens. Matter* **9** 5751–64
[32] Visscher W M, Migliori A, Bell T M and Reinert R A 1991 On the normal modes of free vibration of inhomogeneous and anisotropic elastic objects *J. Acoust. Soc. Am.* **90** 2154
[33] Flügge W 1972 *Tensor Analysis and Continuum Mechanics* (Berlin: Springer)
[34] Ledbetter H M and Naimon E R 1974 *J. Phys. Chem. Ref. Data* **3** 897
Neighbours J R and Alers G A 1958 *Phys. Rev.* **111** 707
Materials Design Elastic Properties of Diamond http://materialsdesign.com/appnote/elastic-properties-diamond
[35] Love A E H 1944 *A Treatise on the Mathematical Theory of Elasticity* 4th edn (New York: Dover Publications) 452 cht. XXI
[36] Charnley T, Perrin R, Mohanan V and Banu H 1989 Vibrations of thin rings of rectangular cross-section *J. Sound Vib.* **134** 455–88